A Robust Estimation of Lorentz Invariance Violation and Intrinsic Spectral Lag of Short Gamma-Ray Bursts

Shuo Xiao[1,2] , Shao-Lin Xiong[1] , Yue Wang[1,3], Shuang-Nan Zhang[1] , He Gao[4] , Zhen Zhang[1] , Ce Cai[1,2], Qi-Bin Yi[1,5],
Yi Zhao[1,4], You-Li Tuo[1] , Xin-Qiao Li[1] , Xiang-Yang Wen[1], Zheng-Hua An[1], Wen-Xi Peng[1], Shi-Jie Zheng[1], Fan Zhang[1],
Li-Ming Song[1] , and Ti-Pei Li[1,6]

[1] Key Laboratory of Particle Astrophysics, Institute of High Energy Physics, Chinese Academy of Sciences, Beijing 100049, People's Republic of China
xiongsl@ihep.ac.cn
[2] University of Chinese Academy of Sciences, Chinese Academy of Sciences, Beijing 100049, People's Republic of China
[3] School of Physics and Astronomy, Yunnan University, 650091 Kunming, People's Republic of China
[4] Department of Astronomy, Beijing Normal University, Beijing 100875, People's Republic of China
[5] Key Laboratory of Stellar and Interstellar Physics and Department of Physics, Xiangtan University, 411105 Xiangtan, Hunan Province, People's Republic of China
[6] Department of Astronomy, Tsinghua University, Beijing 100084, People's Republic of China

Abstract

Gamma-ray bursts (GRBs) have been identified as one of the most promising sources for Lorentz invariance violation (LIV) studies due to their cosmological distance and energetic emission in wide energy bands. However, the arrival-time difference of GRB photons among different energy bands is affected not only by the LIV effect but also by the poorly known intrinsic spectral lags. In previous studies, assumptions of spectral lag have to be made which could introduce systematic errors. In this paper, we used a sample of 46 short GRBs (SGRBs), whose intrinsic spectra lags are much smaller than long GRBs, to better constrain the LIV. The observed spectral lags are derived between two fixed energy bands in the source rest frame rather than the observer frame. Moreover, the lags are calculated with the novel Li–CCF method, which is more robust than traditional methods. Our results show that, if we consider LIV as a linear energy dependence of the photon propagation speed in the data fit, then we obtain a robust limit of $E_{QG} > 10^{15}$ GeV (95% CL). If we assume no LIV effect in the keV–MeV energy range, the goodness of data fit is equivalently as well as the case with LIV and we can constrain the common intrinsic spectral lags of SGRBs to be 1.4 ± 0.5 ms (1σ), which is the most accurate measurement thus far.

Unified Astronomy Thesaurus concepts: Gamma-ray bursts (629)

1. Introduction

The Lorentz invariance violation (LIV) is predicted as the propagation speed of photons being energy dependent possibly around the Planck energy scale $E_p = \sqrt{\hbar c^5/G} \simeq 1.22 \times 10^{19}$ GeV in many quantum gravity (QG) theories (e.g., Kostelecký & Samuel 1989; Kostelecký & Potting 1995; Tasson 2014). Because of their cosmological distances and emission in wide energy bands, gamma-ray bursts (GRBs) are believed to be one of the most promising sources for LIV tests (Amelino-Camelia et al. 1998).

GRBs can be divided into two classes according to their duration and hardness, long GRBs (LGRBs) and short GRBs (SGRBs), which are widely believed to originate from massive-star core collapse and binary neutron star or neutron star–black hole mergers (Woosley & Bloom 2006; Abbott et al. 2017), respectively. Spectral lag of the low-energy photons (i.e., light curve) with respect to the high-energy ones is a well-known phenomenon of GRBs. It is conventionally defined as positive when high-energy photons precede low-energy photons. Long GRBs usually have significantly larger positive or negative spectral lags (e.g., Chen et al. 2005; Ukwatta et al. 2012; Bernardini et al. 2014) than short GRBs. There are a number of proposed interpretations for the observed spectral lag, such as the synchrotron cooling effect (Kazanas et al. 1998) and

kinematic effect due to observing the GRB jet at a large viewing angle (e.g., Sari & Piran 1997; Dermer 2004), both of which can manifest as the observed spectral evolution of the GRB prompt emission (e.g., Kocevski & Liang 2003).

Another possible explanation for the spectral lags is QG effects. Thus, spectral lags have been widely used to investigate the possible LIV effect. Some limits on LIV have been obtained based on the observed time lag of very high energy photons in single GRBs (e.g., Abdo et al. 2009a, 2009b; Acciari et al. 2020). However, for single bursts, it is difficult to disentangle the LIV effect from intrinsic spectral lag which is usually unknown (Bernardini et al. 2017). To partly mitigate this problem, Ellis et al. (2006) proposed fitting the observed spectral lags of a sample of GRBs (mostly LGRBs) with the assumption of a constant intrinsic spectral lag in the rest frame for all GRBs, but this assumption can hardly hold because the intrinsic lag is very likely different among LGRBs. As a result, an additional systematic error (e.g., up to about 54 ms) had to be added in the data fit due to the large reduced χ^2 (e.g., about 4.5) in these kinds of studies. Bernardini et al. (Bernardini et al. 2017) used 15 SGRBs, which are considered to have smaller spectral lags than LGRBs (Norris et al. 2001; Bernardini et al. 2014) to constrain the LIV via two fixed energy bands in the observer frame, but these energy bands correspond to different energies in the source rest frame because different GRBs have different redshifts (Ukwatta et al. 2012; Bernardini et al. 2014; Wei & Wu 2017), which can potentially introduce an artificial energy dependence to the extracted spectral lag and a systematic uncertainty to the limit for LIV (Wei & Wu 2021).

Wei et al. (Wei & Wu 2017) proposed constraining the LIV via two fixed energy bands in the rest frame, however, they mainly used LGRBs rather than SGRBs.

By contrast, Wei et al. (Wei et al. 2017; Du et al. 2020) used those GRBs with a turnover feature in the spectral lag and approximated the observer-frame relation of the intrinsic spectral lag and the energy band as a power law with positive dependence, to constrain the QG energy scale, however, the goodness of the data fitting is not very satisfied (the reduced χ^2 is about 2.2; Ganguly & Desai 2017). Besides, the power-law relations usually exist only in long GRBs with a single pulse (Shao et al. 2017), and it has been found that spectral lag varies between pulses in a single burst (e.g., Hakkila et al. 2008; Zhang 2012). Therefore, using long GRBs to study LIV has unavoidable problems due to the difficulties determining their intrinsic spectral lag which depends on models.

The cross correlation function (CCF) or the discrete cross correlation function (Band 1997) is widely used to calculate spectral lags in previous studies. However, since the time resolution of CCF is almost constrained to the time-bin size of light curves, higher time-resolution results can only be achieved by fitting various functions (e.g., Gaussian, asymmetric Gaussian, polynomial, and parabolic functions) to CCF, during which additional errors could be introduced (e.g., Chen et al. 2005; Yi et al. 2006; McBreen et al. 2008; Bernardini et al. 2014) because the shape of CCF depends on the details of light curves and a simple fitting could usually be insufficient. Besides this, the spectral lags will depend on the chosen function shape and the range of the fit. Finally, since the CCF uses only one light curve, it does not take full advantage of the data with high temporal resolution (e.g., 100 μs for BAT Sakamoto et al. 2008, 2 μs for GBM Meegan et al. 2009 and HXMT/HE Xiao et al. 2020; Liu et al. 2020, and 0.1 μs for GECAM (S. Xiao et al., in preparation)). The improved Li–CCF method (i.e., MCCF; Li et al. 2004; Xiao et al. 2021) can make better use of the temporal information in the high-resolution data, and thus yield more accurate results. In particular, the Li–CCF method can directly calculate the high-resolution time lag without fitting or interpolation of the CCF curve, which avoids the possible bias introduced by the fitting process.

In this paper, we collected a large sample of SGRBs observed by Swift/BAT or Fermi/GBM with redshift measurements (Section 2.1) and used the novel Li–CCF method (Section 2.2) to calculate the spectral lag between two fixed energy ranges at the source rest frame. We used this SGRB sample to test LIV under different models and constrain lower limits of QG energy scale, respectively (Sections 3.1 and 3.2). Finally, discussion and summary of the results are given.

2. Sample Selection and Methodology

2.1. Sample Selection

We collected a sample of SGRBs with redshift measurements observed by Swift/BAT or Fermi/GBM from 2004 November to 2020 December. We mainly refer to the reports from the Swift Burst Analyser (Evans et al. 2009), Fermi GBM Burst Catalog (von Kienlin et al. 2020), and GCN circulars of the Swift and GBM teams. In addition to selecting SGRBs with T90 <2 s, we also include several samples of SGRBs with T90 >2 s reported in the literature (Bromberg et al. 2013; d'Avanzo et al. 2014; Bernardini et al. 2017; Goldstein et al. 2017;

Margutti & Chornock 2021). It is worth noting that the measured duration of GRBs can vary among different instruments (Bromberg et al. 2013). By default, we use the T90 and spectral lag reported by BAT except that there are only GBM results available to use. Our SGRB samples are listed in Table 1.

2.2. Calculation of Spectral Lags

The redshift distribution of SGRBs in the sample ranges from 0.0098 to 2.6. For each GRB, the fixed rest-frame energy bands are selected to be 15–70 keV and 120–250 keV, with the corresponding energy bands in the observer frame being [15–70]/(1+z) and [120–250]/(1+z), respectively. The purpose of the above selection of energy bands is to make the best use of the data (the detection energy range of BAT is about 15–200 keV Sakamoto et al. 2011) and ensure sufficient energy difference between these two bands. We first extract the background-subtracted initial light curves with time bin of 0.5 ms (considering both the accuracy and time consumption of calculation as well as the time resolution of BAT) and their errors with the *batbinevt* command in FTOOLS for two observer-frame energy bands.

Based on the high time-resolution initial light curves ($x(j; \delta t)$ and $y(j; \delta t)$) of Swift/BAT or Fermi/GBM, we utilize the Li–CCF method (see Li et al. 2004 and Xiao et al. 2021 for details) to calculate the spectral lags, which is defined as

$$
\begin{aligned}
\mathrm{MCCF}(k, \Delta t) &= \frac{1}{M_{\Delta t}} \sum_{m=1}^{M_{\Delta t}} \\
&\quad \sum_i u_m(i; \Delta t) v_{m+k}(i; \Delta t) / \sigma_u \sigma_v.
\end{aligned}
\tag{1}
$$

Where the combination starts from the mth bin of the initial light curves, the phase factor $m = 1, 2, \cdots, M_{\Delta t}$, and $u_m(\Delta t)$ and $v_m(\Delta t)$ are the background-subtracted series of $x_m(\Delta t)$ and $y_m(\Delta t)$ by re-binning the initial series, we obtain the light curves with an optimized time bin $\Delta t = M_{\Delta t} \delta t$ (from 1 to 100 ms for SGRBs, from 1 ms to 1 s for LGRBs), respectively,

$$
\begin{aligned}
u_m(i; \Delta t) &= x_m(i; \Delta t) - b_{x_m}(i; \Delta t), \\
v_m(i; \Delta t) &= y_m(i; \Delta t) - b_{y_m}(i; \Delta t), \\
\sigma_u^2 &= \sum_i u_m(i; \Delta t)^2, \\
\sigma_v^2 &= \sum_i v_m(i; \Delta t)^2,
\end{aligned}
\tag{2}
$$

where b_{x_m} and b_{y_m} are the background counts of light curves $x_m(\Delta t)$ and $y_m(\Delta t)$, respectively. We can find a value $k_{\max}$ of k that maximizes $\mathrm{MCCF}(k = k_{\max}, \Delta t)$, then the relative time lag between two light curves $y_m(i; \Delta t)$ and $x_m(i; \Delta t)$ on Δt is

$$
\tau(\Delta t) = k_{\max} \delta t.
\tag{3}
$$

To obtain the uncertainty, we implement a Monte Carlo (MC) simulation of the observed light curves based on a Gaussian (for BAT) or Poisson (for GBM) probability distribution (see Xiao et al. 2021 for details). Since the distribution can be approximated as a Gaussian distribution in most cases, we use the standard deviation of the distribution as the standard deviation of the Gaussian distribution. Note that, although the distribution may not behave like a Gaussian when the signals of the light curves are weak, the effect on subsequent fits in the analysis can be neglected since the

Table 1
Spectral Lags of 46 SGRBs with Redshift Measurements at Fixed Energy Bands (15–70 keV and 120–250 keV) in the Source Rest Frame

Name	z	T90	α (PL)	$E_{l'}$ (keV)	$E_{h'}$ (keV)	$\Delta t_{\rm BAT}$	$\sigma_{\rm BAT}$	$\Delta t_{\rm GBM}$	$\sigma_{\rm GBM}$
201221D	1.045	0.16	1.56 ± 0.13	7–34	59–122	0.005	0.006	0.009	0.008
200826A	0.748	1.14	⋯	9–40	69–143	⋯	⋯	0.017	0.009
200522A	0.554	0.62	1.45 ± 0.17	10–45	77–161	0.024	0.039	⋯	⋯
190627A	1.942	1.60	2.38 ± 0.38	5–24	41–85	0.205	0.265	⋯	⋯
181123B	1.754	0.26	0.72 ± 0.28	5–25	44–91	0.07	0.092	⋯	⋯
170817A	0.0098	2.05	1.80 ± 0.10	15–69	119–248	⋯	⋯	0.174	0.117
170428A	0.454	0.20	0.76 ± 0.12	10–48	83–172	0.008	0.007	⋯	⋯
160821B	0.160	0.48	1.88 ± 0.15	13–60	103–216	0.082	0.3	0.013	0.167
160624A	0.483	0.20	0.57 ± 0.45	10–47	81–169	0.005	0.093	−0.007	0.16
160410A	1.718	8.20	0.93 ± 0.17	6–26	44–92	0.009	0.193	⋯	⋯
150423A	1.394	0.22	0.84 ± 0.24	6–29	50–104	−0.013	0.039	⋯	⋯
150120A	0.460	1.20	1.81 ± 0.18	10–48	82–171	0.349	0.316	−0.207	0.297
150101B	0.134	0.02	3.30 ± 0.50	13–62	106–220	0.009	0.082	0.006	0.012
140903A	0.351	0.30	1.99 ± 0.12	11–52	89–185	−0.003	0.07	⋯	⋯
140622A	0.959	0.13	3.08 ± 0.33	8–36	61–128	−0.035	0.148	⋯	⋯
131004A	0.717	1.54	1.81 ± 0.11	9–41	70–146	0.181	0.089	0.14	0.114
130603B	0.356	0.18	0.82 ± 0.07	11–52	88–184	0	0.001	⋯	⋯
120804A	1.300	0.81	1.34 ± 0.08	7–30	52–109	0.027	0.025	⋯	⋯
111117A	2.211	0.47	0.65 ± 0.22	5–22	37–78	0.004	0.223	0.034	0.262
101219A	0.718	0.60	0.63 ± 0.09	9–41	70–146	0.019	0.012	⋯	⋯
100724A	1.288	1.40	1.92 ± 0.21	7–31	52–109	0.343	0.199	⋯	⋯
100628A	0.102	0.04	1.25 ± 0.26	14–64	109–227	−0.004	0.078	⋯	⋯
100625A	0.452	0.33	0.90 ± 0.10	10–48	83–172	−0.001	0.022	0.018	0.046
100206A	0.407	0.12	0.63 ± 0.17	11–50	85–178	−0.01	0.011	−0.003	0.007
100117A	0.915	0.30	0.88 ± 0.22	8–37	63–131	−0.001	0.047	−0.034	0.102
090510	0.903	0.30	0.98 ± 0.20	8–37	63–131	−0.005	0.016	−0.004	0.006
090426	2.609	1.20	1.93 ± 0.22	4–19	33–69	−0.042	0.178	⋯	⋯
080905A	0.122	1.00	0.85 ± 0.24	13–62	107–223	0.163	0.094	0.11	0.204
080123	0.495	0.80	2.15 ± 0.54	10–47	80–167	0.012	0.014	⋯	⋯
071227	0.381	1.80	0.99 ± 0.22	11–51	87–181	−0.043	0.19	⋯	⋯
070809	0.219	1.30	1.69 ± 0.22	12–57	98–205	0.101	0.315	⋯	⋯
070724A	0.457	0.40	1.81 ± 0.33	10–48	82–172	−0.013	0.261	⋯	⋯
070714B	0.923	3.00	1.36 ± 0.19	8–36	62–130	0.015	0.007	⋯	⋯
070429B	0.904	0.47	1.72 ± 0.23	8–37	63–131	0.366	0.221	⋯	⋯
061217	0.827	0.21	0.86 ± 0.30	8–38	66–137	0.066	0.072	⋯	⋯
061210	0.410	0.19	1.56 ± 0.28	11–50	85–177	0.004	0.002	⋯	⋯
061201	0.111	0.76	0.81 ± 0.15	14–63	108–225	−0.017	0.15	⋯	⋯
061006	0.438	0.50	1.72 ± 0.17	10–49	83–174	0.036	0.008	⋯	⋯
060801	1.131	0.49	0.47 ± 0.24	7–33	56–117	−0.012	0.045	⋯	⋯
060502B	0.287	0.13	0.98 ± 0.19	12–54	93–194	0.01	0.03	⋯	⋯
060313	0.750	0.74	0.70 ± 0.07	9–40	69–143	0.003	0.002	⋯	⋯
051221A	0.546	1.40	1.39 ± 0.06	10–45	78–162	0.002	0.001	⋯	⋯
051210	1.300	1.30	1.06 ± 0.28	7–30	52–109	0.316	0.288	⋯	⋯
050813	0.722	0.45	1.28 ± 0.37	9–41	70–145	−0.043	0.074	⋯	⋯
050724	0.257	3.00	1.89 ± 0.22	12–56	95–199	−0.013	0.061	⋯	⋯
050509B	0.225	0.07	1.57 ± 0.38	12–57	98–204	0.006	0.128	⋯	⋯

Note. The units of T90, Δt, and σ are in seconds. The T90 is the result of BAT by default. The redshift z and spectral index α are from the Swift Burst Analyser (Evans et al. 2009), Fermi GBM Burst Catalog (von Kienlin et al. 2020), and GCN circulars of the Swift and GBM teams.

errors are usually larger in this case. The probability distribution of the spectral lag for the ith GRB in the sample is

$$p(i; \Delta t_{\rm mod}) = \frac{1}{\sqrt{2\pi}\, \sigma_{\Delta t_{\rm obs}}}$$
$$\times \exp\left[-\frac{(\Delta t_{\rm obs} - \Delta t_{\rm mod})^2}{2(\sigma_{\Delta t_{\rm obs}})^2} \right], \qquad (4)$$

where $\Delta t_{\rm obs}$ and $\sigma_{\Delta t_{\rm obs}}$ are the observed spectral lag and its error (see Table 1), respectively. The $\Delta t_{\rm mod}$ is the expected value according to the model (Section 2.3). As shown in Table 1, the spectral lags are calculated in different energy bands in the

observer frame which corresponds to the fixed energy bands in the source rest frame.

2.3. LIV Constraints

The speed of propagation of photons of energy (E) due to LIV can be described by a Taylor expansion as

$$E^2 \simeq p^2 c^2 \left[1 - s_{\pm} \left(\frac{pc}{E_{\rm QG,n}} \right)^n \right], \qquad (5)$$

where $E_{\rm QG,n}$ is the QG energy scale, s for $+1$ and $−1$ represent whether the high-energy photons are slower or faster than the

low-energy ones, respectively. The n represents whether it is linear ($n = 1$) or quadratic ($n = 2$) energy dependence. And a photon propagation speed is

$$v = \frac{\partial E}{\partial p} \approx c \left[1 - s_\pm \frac{n+1}{2} \left(\frac{E}{E_{QG,n}} \right) \right]. \quad (6)$$

Due to the cosmological expansion, the LIV induced observed time lag is (Jacob & Piran 2008; Zhang & Ma 2015)

$$\Delta t_{LIV} = -s_\pm \frac{1+n}{2H_0} \frac{E_h^n - E_l^n}{(1+z)^n E_{QG,n}^n} \int_0^z \frac{(1+z')^n dz'}{h(z')}, \quad (7)$$

where H_0 is the Hubble constant, and $h(z) = \sqrt{\Omega_m (1+z)^3 + \Omega_\Lambda}$, which is the dimensionless Hubble expansion rate at z, we use the standard flat ΛCDM model ($H_0 = 67.8$ kms^{-1} Mpc^{-1}, $\Omega_m = 0.308$, and $\Omega_\Lambda = 1 - \Omega_m = 0.692$). It is worth noting that E_h and E_l are the higher and lower rest-frame energies (source frame), respectively.

Meanwhile, we assume that all GRBs have the same intrinsic spectral lag, b, in the rest frame of the source at redshift z as in the previous studies (e.g., Ellis et al. 2006; Wei & Wu 2017),

$$\Delta t_{obs} = \Delta t_{LIV} + b(1+z), \quad (8)$$

where $(1+z)$ is the correction for the time-dilation effect. Since E_h and E_l are fixed (i.e., 15–70 keV and 120–250 keV), for subsequent analysis, we can re-express Equation (7) as

$$\frac{\Delta t_{obs}}{1+z} = a_{LIV}(s, n, E_{QG})K(z) + b, \quad (9)$$

where $K(z)$ is a function of the redshift only,

$$K(z) = \frac{1}{(1+z)^{n+1}} \int_0^z \frac{(1+z')^n dz'}{h(z')}, \quad (10)$$

and $a(s, n, E_{QG})$ is a function of the parameters to be estimated

$$a_{LIV}(s, n, E_{QG}) = -s_\pm \frac{1+n}{2H_0} \frac{E_h^n - E_l^n}{E_{QG,n}^n}, \quad (11)$$

The $E_{QG,n}^n$ is calculated by the maximum likelihood estimation method. The likelihood function is

$$\mathcal{L}(\theta) = \prod_i p(i; \Delta t_{mod}(\theta)), \quad (12)$$

where p is the probability distribution of the spectral lag (Equation (4)), and θ is the free parameters (e.g., a_{LIV} and b).

To obtain the lower limit, we employed the procedure proposed by Ellis et al. (Ellis et al. 2006). Marginalizing the likelihood function over the intercept parameters, the 95% confidence limit on the scale $E_{QG,n}$ by solving the equation

$$\frac{\int_{E_{QG,n}}^{E_\infty} \mathcal{L}_{marg}(E) dE}{\int_0^{E_\infty} \mathcal{L}_{marg}(E) dE} = 0.95, \quad (13)$$

where E_∞ is a reference point fixing the normalization and we choose the $E_\infty = 1.22 \times 10^{19}$ GeV, which is Planck energy scale.

3. Quantum Gravity Energy-scale Limits

3.1. For n = 1 Linear Energy Dependence

The calculated spectral lags Δt_{obs} and their uncertainties $\sigma_{\Delta t_{obs}}$ results are shown in Table 1. We plot the $\Delta t_{obs}/(1+z)$ versus K(z) in Figure 1, and perform a linear fit $\Delta t_{obs}/(1+z) = \Delta t_{LIV}/(1+z) + b = a_{LIV}K(z) + b$.

The best-fit $a_{LIV} = 0.027 \pm 0.020$ and $b = -0.005 \pm 0.005$ s are obtained via the Markov Chain Monte Carlo (MCMC), and the Akaike information criterion (AIC; Akaike 1974) and the Bayesian information criterion (BIC; Schwarz 1978) are −191 and −188, respectively. The reduced χ^2 is 50/44 = 1.15. The fitting results are shown in Figure 1. It is worth noting that the correlation coefficient between a_{LIV} and b is −0.996, which means that it leads to larger errors (Barlow 1993).

In addition, we performed the fits using $\Delta t_{obs} = \Delta t_{LIV}$ (ignoring the intrinsic spectral lags) and $\Delta t_{obs}/(1+z) = b$ (no LIV, see Figure 1), respectively, and the results are listed in Table 2. Since no fit is significantly better than others, we choose to be conservative in estimating LIV using the fit obtained by $\Delta t_{obs} = \Delta t_{LIV} + b(1+z)$.

According to Equations (11) and (13), for $n = 1$ and $s = -1$, which is linear energy dependence, the speed of higher-energy photons is faster. We calculate the 95% confidence level lower limit of E_{QG} as

$$E_{QG,n=1} \geqslant 1.0 \times 10^{15} \text{ GeV}. \quad (14)$$

For $n = 1$ and $s = +1$, the 95% confidence level lower limit of E_{QG} is

$$E_{QG,n=1} \geqslant 2.5 \times 10^{15} \text{ GeV}. \quad (15)$$

3.2. For n = 2 Quadratic Energy Dependence

We perform a linear fit $\Delta t_{obs}/(1+z) = \Delta t_{LIV}/(1+z) = a_{LIV}K(z) + b$ for $n = 2$. The best-fit $a_{LIV} = 0.039 \pm 0.038$ and $b = -0.006 \pm 0.008$ is obtained via MCMC, and the AIC and BIC are −191 and −187, respectively. The reduced χ^2 is 51/44 = 1.16.

For $n = 2$ and $s = -1$, the 95% confidence level lower limit of E_{QG} is

$$E_{QG,n=2} \geqslant 0.9 \times 10^6 \text{ GeV}. \quad (16)$$

For $n = 2$ and $s = +1$, the 95% confidence level lower limit of E_{QG} is

$$E_{QG,n=2} \geqslant 1.2 \times 10^6 \text{ GeV}. \quad (17)$$

4. Discussion and Conclusion

We collected a large sample of 46 SGRBs with redshift measurements observed by Swift/BAT or Fermi/GBM from 2005 to 2020, and extracted spectral lags between light curves in two fixed energy bands in the source rest frame, employing the novel improved Li–CCF method. Because Li–CCF makes use of more temporal information contained in the observed light curve and does not need to assume the shape of the CCF to fit, it can avoid possible bias in the calculated spectral lags which otherwise would be introduced during the fit process in traditional methods. Thus, the observed spectral lags given by Li–CCF is more accurate and robust.

Since different instruments have different energy responses, to verify whether the spectral lags are instrument-dependent, we examined the SGRBs with redshift measurements observed
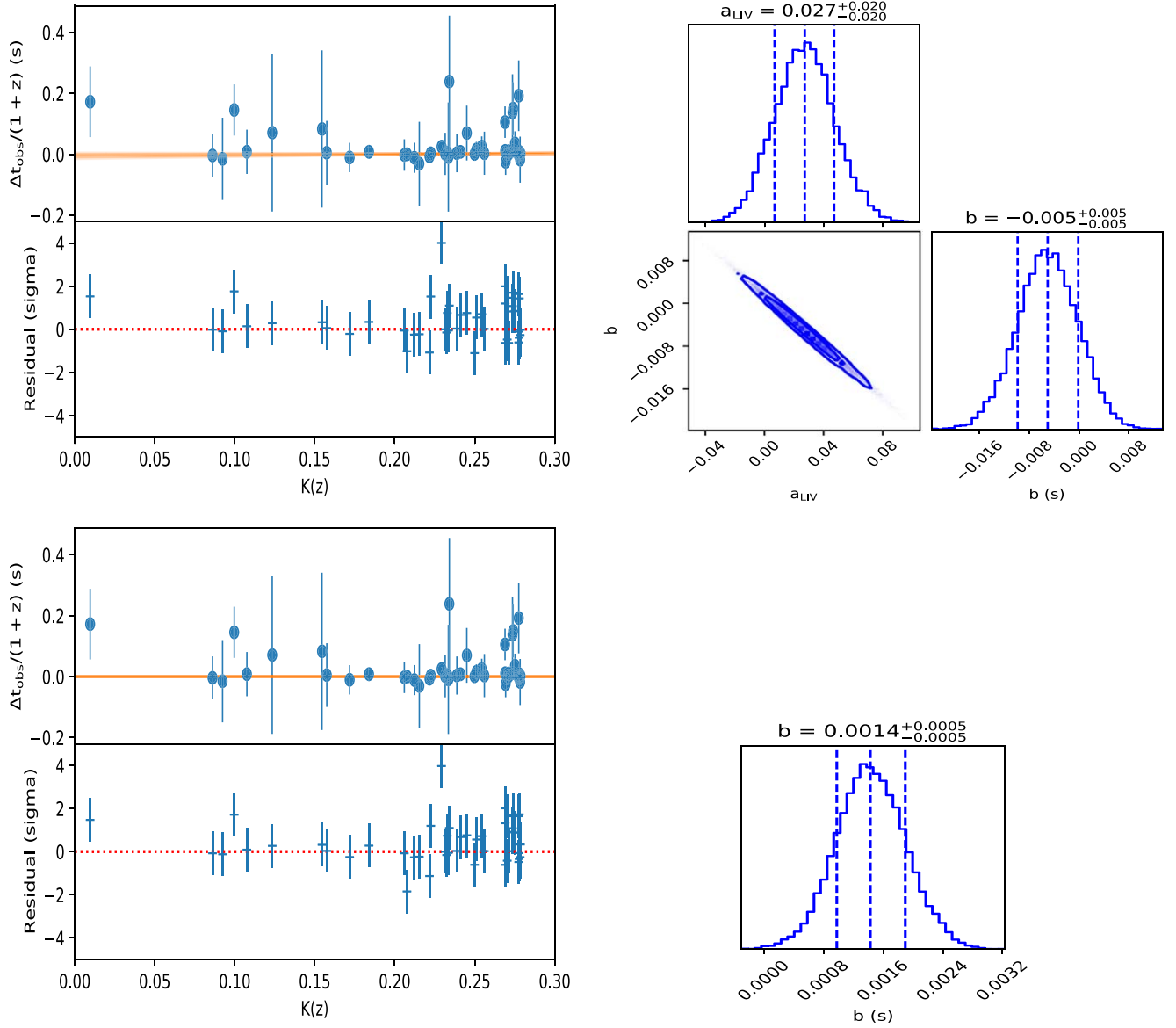
Figure 1. (Top left panel) The $\Delta t_{\mathrm{obs}}/(1+z)$ as a function of K(z). The yellow region is obtained by fitting $\Delta t_{\mathrm{obs}}/(1+z) = \Delta t_{\mathrm{LIV}}/(1+z) + b = a_{\mathrm{LIV}}K(z) + b$. (Top right panel) The corresponding fit results obtained by MCMC. The correlation coefficient between a_{LIV} and b is -0.996. (Bottom left panel) The yellow region is obtained by fitting $\Delta t_{\mathrm{obs}}/(1+z) = b$ (i.e., assuming no LIV). (Bottom right panel) The corresponding fit result obtained by MCMC assuming no LIV effect.

Table 2
Comparison of Models Based on AIC, BIC, and Reduced χ^2 ($n = 1$)

Model	Parameters	AIC	BIC	χ^2/dof	E_{QG} ($s = -1$)	E_{QG} ($s = +1$)
$\Delta t_{\mathrm{obs}} = b(1+z)$ (No LIV)	$b = 1.4 \pm 0.5$ ms	-192	-190	1.16	$+\infty$	$+\infty$
$\Delta t_{\mathrm{obs}} = \Delta t_{\mathrm{LIV}}$	$a_{\mathrm{LIV}} = 0.006 \pm 0.002$	-192	-191	1.15	$\geqslant 0.7 \times 10^{16}$ GeV	$\geqslant 0.4 \times 10^{17}$ GeV
$\Delta t_{\mathrm{obs}} = \Delta t_{\mathrm{LIV}} + b(1+z)$	$a_{\mathrm{LIV}} = 0.027 \pm 0.020$, b $= -5.0 \pm 5.2$ ms	-191	-187	1.15	$\geqslant 1.0 \times 10^{15}$ GeV	$\geqslant 2.5 \times 10^{15}$ GeV

Note. The reported error of parameters is for 1σ, and the E_{QG} is the lower limit with 95% CL. *Where b is the intrinsic spectral lags in the source rest frame, a_{LIV} is a function of E_{QG} (Equation (11)).

jointly by Swift/BAT and Fermi/GBM, and calculated the spectral lags between two fixed energy ranges (i.e., 15–70 keV and 120–250 keV) in the source rest frame for the NaI detector of Fermi/GBM. The results are shown in Figure 2, which can confirm that the spectral lags of SGRBs obtained by GBM and BAT are consistent with zero within the error range. For the 46 SGRBs samples used, only two of them are GBM data; the other 44 are BAT. This also avoids possible systematic errors caused by

different instruments. Furthermore, we use only BAT or GBM data to fit with $\Delta t_{\mathrm{obs}} = \Delta t_{\mathrm{LIV}} + b(1+z)$, respectively, and the results are $a_{\mathrm{LIV}} = 0.023 \pm 0.021$, $b = -0.004 \pm 0.005$ and $a_{\mathrm{LIV}} = 0.022 \pm 0.036$, $b = -0.005 \pm 0.009$ s. The reduced χ^2 are $46/42 = 1.10$ and $10/12 = 0.88$, respectively. Therefore, the results obtained by GBM or BAT, respectively, are consistent within the error range. However, we calculated the spectral lags between the same energy ranges in the source rest frame for 21
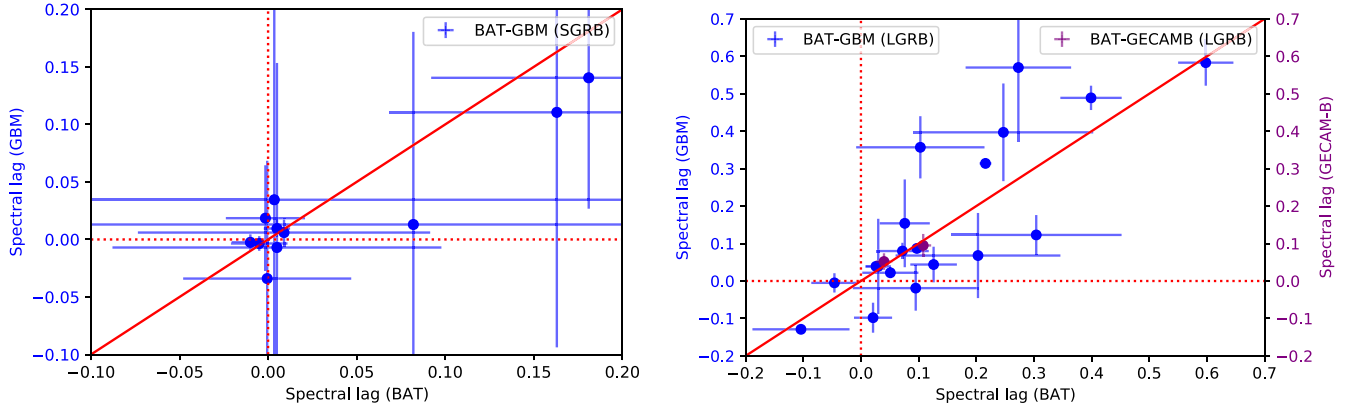
Figure 2. Spectral lags of SGRBs observed jointly by BAT-GBM are shown in the left panel. The right panel shows the spectral lags of the LGRBs observed by BAT-GECAMB and BAT-GBM. Both are 15–70 keV compared to 120–250 keV in the source rest frame.

Table 3
Spectral Lags of 21 Bright LGRBs with Redshift Measurements at Fixed Energy Bands (15–70 keV and 120–250 keV) in the Source Rest Frame

Name	z	T90	α (PL)	$E_{l'}$ (keV)	$E_{h'}$ (keV)	Δt_{BAT}	σ_{BAT}	Δt_{GBM}	σ_{GBM}	Δt_{GECAM}	σ_{GECAM}
210822A	1.736	181	1.30 ± 0.4	5–26	44–91	0.04	0.015	⋯	⋯	0.052	0.022
210619B	1.937	61	1.41 ± 0.02	5–24	41–85	0.108	0.014	⋯	⋯	0.095	0.031
190719C	2.469	186	1.64 ± 0.09	4–20	35–72	0.273	0.091	0.57	0.198	⋯	⋯
190114C	0.425	362	1.43 ± 0.02	11–49	84–175	0.097	0.006	0.087	0.004	⋯	⋯
181020A	2.938	238	1.25 ± 0.06	4–18	30–63	0.203	0.143	0.068	0.114	⋯	⋯
180728A	0.117	9	1.97 ± 0.03	13–63	107–224	−0.104	0.084	−0.129	0.009	⋯	⋯
180720B	0.654	108	1.36 ± 0.03	9–42	73–151	0.026	0.018	0.039	0.004	⋯	⋯
170705A	2.010	217	1.65 ± 0.05	5–23	40–83	0.076	0.043	0.154	0.117	⋯	⋯
151027A	0.810	130	1.72 ± 0.05	8–39	66–138	0.103	0.111	0.357	0.083	⋯	⋯
150403A	2.060	41	1.23 ± 0.04	5–23	39–82	0.247	0.156	0.397	0.13	⋯	⋯
150314A	1.758	15	1.08 ± 0.03	5–25	44–91	0.399	0.053	0.489	0.032	⋯	⋯
141220A	1.320	7	1.30 ± 0.08	6–30	52–108	0.095	0.109	−0.019	0.06	⋯	⋯
141004A	0.573	4	1.86 ± 0.08	10–45	76–159	0.021	0.033	−0.098	0.04	⋯	⋯
140512A	0.725	155	1.45 ± 0.04	9–41	70–145	0.072	0.046	0.08	0.022	⋯	⋯
140506A	0.889	111	1.68 ± 0.16	8–37	64–132	0.304	0.148	0.123	0.053	⋯	⋯
140213A	1.208	60	1.80 ± 0.04	7–32	54–113	−0.046	0.04	−0.005	0.026	⋯	⋯
130427A	0.340	163	1.21 ± 0.02	11–52	90–187	0.216	0.01	0.314	0.005	⋯	⋯
121128A	2.200	23	1.32 ± 0.18	5–22	38–78	0.03	0.022	0.039	0.127	⋯	⋯
111228A	0.714	101	2.27 ± 0.06	9–41	70–146	0.051	0.049	0.022	0.014	⋯	⋯
100728A	1.567	199	1.18 ± 0.02	6–27	47–97	0.126	0.04	0.044	0.048	⋯	⋯
090618	0.540	113	1.58 ± 0.02	10–45	78–162	0.598	0.048	0.583	0.062	⋯	⋯

Note. The units of T90, Δt, and σ are in seconds. The T90 default is the result of using BAT measurements. The redshift z and α are from the Swift Burst Analyser (Evans et al. 2009), Fermi GBM Burst Catalog (von Kienlin et al. 2020), and GCN circulars of the Swift and GBM teams.

bright long GRBs observed by BAT-GBM and BAT-GECAMB and found that most of them are significantly nonzero, which is also consistent with the findings of previous studies (see Table 3; Bernardini et al. 2014). In addition, we find that the spectral lags of BAT and GBM are not in perfect one-to-one relation, which may be due to the different incident angles of the detectors on GBM for different GRBs, resulting in different energy responses. In contrast, since GECAM has more detectors (i.e., 25 GRDs) and a more uniform incident angle distribution, its results are in better agreement with those of BAT.

To estimate the systematic effect due to the energy resolution of BAT, the observed energy is shifted by 7 kev, which is based on the energy resolution of BAT (Barthelmy et al. 2005). We find their results are consistent within the error, but the difference in the best value of E_{QG} is about 10%, and the difference in the intrinsic spectral lags obtained for the assumption of no LIV is about 14%. Besides this, the effect of selecting different energy ranges at rest frame is also investigated; we select 50–100 keV

and 150–250 keV and fit with $\Delta t_{obs} = \Delta t_{LIV} + b(1 + z)$ and $\Delta t_{obs} = b(1 + z)$, respectively. The results are $a_{LIV} = 0.001 \pm 0.027$, $b = 0.001 \pm 0.007$ s and $b = 1.1 \pm 0.5$ ms, respectively, which means that they are consistent with the results obtained for 15–70 keV and 120–250 keV within the error range. Therefore, for BAT, which is mainly used in our work, the energy range that can be selected is small due to its narrow observed energy range (15–150 keV), and the results obtained by different energy ranges are consistent within the error range and do not improve significantly.

Based on the observed spectral lags of this large sample of SGRBs, we tested the LIV effects and made an estimation of the common intrinsic spectral lags of SGRBs (if assuming all SGRBs have the same intrinsic spectral lag). The results obtained by fitting with $\Delta t_{obs} = \Delta t_{LIV} + b(1 + z)$ show a strong negative correlation (i.e., $\rho = -0.996$) between Δt_{LIV} and b, which leads to large errors on both of them. However, in this paper, we take this result conservatively without rescaling

by a factor $\sqrt{1-\rho^2}$ as in some previous studies (e.g., Ellis et al. 2006, with the exception of Wei et al. Wei & Wu 2017), and directly use the results obtained from MCMC to calculate the lower limits of E_{QG}. It is worth noting that, since we are able to fit the data well, there is no need to include a systematic error as done in previous studies (e.g., Ellis et al. 2006; Bernardini et al. 2017; Wei & Wu 2017). Our constraint results for E_{QG} are about five times higher than in Wei et al. (Wei & Wu 2017). Although the E_{QG} limits obtained by fitting a sample of GRBs are less stringent than those obtained with high-energy photons in a single GRB (e.g., Martínez-Huerta et al. 2020), this statistical approach based on many GRBs has the advantage of minimizing intrinsic effects in individual GRBs. Moreover, the goodness of our fitting (the reduced χ^2 is about 1.2) shows that our results are more robust than previous studies in a statistical sense.

Our results also indicate that, if assuming no LIV effect in the keV–MeV energy range, which is also supported by the stringent constraints on LIV from single GRBs (e.g., Abdo et al. 2009a, 2009b), and assuming all SGRBs have the same intrinsic spectral lag, the common intrinsic spectral lags of SGRBs between 15–70 keV and 120–250 keV at the source rest frame is 1.4 ± 0.5 ms (1σ), which is the most accurate measurement thus far. This means that most SGRBs in our sample are consistent with having a very small (in the order of 1 ms) spectral lag (although some bursts have relatively large measurement error on the spectral lag as shown in Table 1 and Figure 1), with a confidence level of about 2.9σ for nonzero lag. In addition, the lag between 50–100 keV and 150–250 keV is slightly smaller than that in the low-energy band (i.e., 15–70 keV and 120–250 keV), which may be due to a "curvature" effect (Zhang et al. 2009). Indeed, we note that a few of the SGRBs in our sample cannot be excluded as the LGRB nature, especially those with nonzero spectral lags and larger power-law index α (hardness is softer; Bromberg et al. 2013). However, since we are using a statistical method of many GRBs to constrain LIV, the impact of this small number of suspected SGRBs on the LIV limit results is negligible.

Apart from having very small or even zero intrinsic spectral lag, SGRBs usually do not show the different spectral lags in different pulses across the burst as LGRBs do. All these suggest that SGRBs are ideal sources for testing the LIV effect. Although the measured spectral lags can be well fitted with $\Delta t_{obs}/(1+z) = b$ assuming that the LIV effect does not exist, if the intrinsic spectral lag is ignored, they can also be well fitted by $\Delta t_{obs} = \Delta t_{LIV}$, considering only the LIV effect.

ORCID iDs

Shuo Xiao ⓘ https://orcid.org/0000-0003-2957-2806
Shao-Lin Xiong ⓘ https://orcid.org/0000-0002-4771-7653
Shuang-Nan Zhang ⓘ https://orcid.org/0000-0001-5586-1017
He Gao ⓘ https://orcid.org/0000-0002-3100-6558
Zhen Zhang ⓘ https://orcid.org/0000-0003-4673-773X
You-Li Tuo ⓘ https://orcid.org/0000-0003-3127-0110
Xin-Qiao Li ⓘ https://orcid.org/0000-0003-3466-9493
Li-Ming Song ⓘ https://orcid.org/0000-0003-0274-3396
Ti-Pei Li ⓘ https://orcid.org/0000-0003-3466-9493

References

Abbott, B. P., Abbott, R., Abbott, T., et al. 2017, ApJL, 848, L13
Abdo, A. A., Ackermann, M., Ajello, M., et al. 2009b, Natur, 462, 331
Abdo, A. A., Ackermann, M., Arimoto, M., et al. 2009a, Sci, 323, 1688
Acciari, V. A., Ansoldi, S., Antonelli, L. A., et al. 2020, PhRvL, 125, 021301
Akaike, H. 1974, ITAC, 19, 716
Amelino-Camelia, G., Ellis, J., Mavromatos, N. E., Nanopoulos, D. V., & Sarkar, S. 1998, Natur, 393, 763
Band, D. L. 1997, ApJ, 486, 928
Barlow, R. J. 1993, Statistics: a guide to the use of statistical methods in the physical sciences, 29 (New York: Wiley)
Barthelmy, S. D., Barbier, L. M., Cummings, J. R., et al. 2005, SSRv, 120, 143
Bernardini, M. G., Ghirlanda, G., Campana, S., et al. 2014, MNRAS, 446, 1129
Bernardini, M. G., Ghirlanda, G., Campana, S., et al. 2017, A&A, 607, A121
Bromberg, O., Nakar, E., Piran, T., et al. 2013, ApJ, 764, 179
Chen, L., Lou, Y.-Q., Wu, M., et al. 2005, ApJ, 619, 983
d'Avanzo, P., Salvaterra, R., Bernardini, M., et al. 2014, MNRAS, 442, 2342
Dermer, C. D. 2004, ApJ, 614, 284
Du, S.-S., Lan, L., Wei, J.-J., et al. 2020, ApJ, 906, 8
Ellis, J., Mavromatos, N. E., Nanopoulos, D. V., Sakharov, A. S., & Sarkisyan, E. K. G. 2006, APh, 25, 402
Evans, P., Beardmore, A., Page, K., et al. 2009, MNRAS, 397, 1177
Ganguly, S., & Desai, S. 2017, APh, 94, 17
Goldstein, A., Veres, P., Burns, E., et al. 2017, ApJL, 848, L14
Hakkila, J., Giblin, T. W., Norris, J. P., Fragile, P. C., & Bonnell, J. T. 2008, ApJL, 677, L81
Jacob, U., & Piran, T. 2008, JCAP, 2008, 031
Kazanas, D., Titarchuk, L. G., & Hua, X.-M. 1998, ApJ, 493, 708
Kocevski, D., & Liang, E. 2003, ApJ, 594, 385
Kostelecký, V. A., & Potting, R. 1995, PhRvD, 51, 3923
Kostelecký, V. A., & Samuel, S. 1989, PhRvD, 39, 683
Li, T.-P., Qu, J.-L., Feng, H., et al. 2004, ChJAA, 4, 583
Liu, C., Zhang, Y., Li, X., et al. 2020, ScChG, 63, 1
Margutti, R., & Chornock, R. 2021, ARA&A, 59, 43
Martínez-Huerta, H., Lang, R. G., & De Souza, V. 2020, Symmetry, 12, 1232
McBreen, S., Foley, S., Watson, D., et al. 2008, ApJL, 677, L85
Meegan, C., Lichti, G., Bhat, P., et al. 2009, ApJ, 702, 791
Norris, J., Scargle, J., Bonnell, J., et al. 2001, in Proc. Int. Workshop held in Rome, Italy, ESO Astrophysics Symp, ed. E. Costa et al. (Berlin: Springer), 40
Sakamoto, T., Barthelmy, S., Barbier, L., et al. 2008, ApJS, 175, 179
Sakamoto, T., Barthelmy, S., Baumgartner, W., et al. 2011, ApJS, 195, 2
Sari, R., & Piran, T. 1997, ApJ, 485, 270
Schwarz, G. 1978, AnSta, 6, 461
Shao, L., Zhang, B.-B., Wang, F.-R., et al. 2017, ApJ, 844, 126
Tasson, J. D. 2014, RPPh, 77, 77062901
Ukwatta, T., Dhuga, K., Stamatikos, M., et al. 2012, MNRAS, 419, 614
von Kienlin, A., Meegan, C., Paciesas, W., et al. 2020, ApJ, 893, 46
Wei, J.-J., & Wu, X.-F. 2017, ApJ, 851, 127
Wei, J.-J., & Wu, X.-F. 2021, FrPhy, 16, 44300
Wei, J.-J., Zhang, B.-B., Shao, L., Wu, X.-F., & Mészáros, P. 2017, ApJL, 834, L13
Woosley, S., & Bloom, J. 2006, ARA&A, 44, 507
Xiao, S., Xiong, S. L., Liu, C. Z., et al. 2020, JHEAp, 26, 58
Xiao, S., Xiong, S. L., Zhang, S. N., et al. 2021, ApJ, 920, 43
Yi, T., Liang, E., Qin, Y., & Lu, R. 2006, MNRAS, 367, 1751
Zhang, B., Zhang, B.-B., Virgili, F. J., et al. 2009, ApJ, 703, 1696
Zhang, F.-W. 2012, Ap&SS, 339, 123
Zhang, S., & Ma, B.-Q. 2015, APh, 61, 108